Publisher's note: This SI document was updated on 11th April 2025 to replace an unrevised version that had been uploaded to the platform in error.

# Supporting Information

## Customizable bistable units for soft-rigid grippers enable handling of multi-feature objects via data-driven design

*Jian He, Yaohui Wang, Hubocheng Tang, Guoquan Zhang, Ke Dong, Dong Wang, Liang Xia*, and Yi Xiong**

J. He, Y. Wang, H. Tang, K. Dong, Y. Xiong

School of System Design and Intelligent Manufacturing, Southern University of Science and Technology, Shenzhen 518055, China.

E-mail: xiongy3@sustech.edu.cn

G. Zhang, K. Dong

Department of Industrial and Systems Engineering, The Hong Kong Polytechnic University, Kowloon, Hong Kong.

D. Wang

State Key Laboratory of Mechanical System and Vibration, School of Mechanical Engineering, Shanghai Jiao Tong University, Shanghai 200240, China.

Meta Robotics Institute, Shanghai Jiao Tong University, Shanghai 200240, China.

L. Xia

State Key Laboratory of Intelligent Manufacturing Equipment and Technology, Huazhong University of Science and Technology, Wuhan, 430074, China.

E-mail: xialiang@hust.edu.cn

In this supplementary document, we provide:

Section S1. Parametrized contact block (CB) model in the bistable units

Section S2. Inverse design of CB model for target transition behaviors

Section S3. Soft-rigid grippers comprising pixel arrays of bistable units

Section S4. Determination of grasping behaviors for soft-rigid grippers

Other supplementary materials for this manuscript include Videos S1 to S3.

**Section S1. Parametrized contact block (CB) model in the bistable units**

We propose a novel class of bistable units capable of modulating transition behaviors (Fig. S1). The shape of the curved beam in these bistable units is defined by the parameterized function $y(x) = -H/2\cos((x/W)^g\pi), x \in [0, W]$. In a previous study, we set $g = 2$, which made the stiffness of the loading end larger than that of the fixed end[1]. Under a uniaxial compression test, the beam at the fixed end initially deforms into a wave trough pattern. To this end, we place CB beneath the curved beam to program the deformation state for tuning transition behaviors. At an applied strain of 0.2, as shown in the right figure of Fig. S1, CB places at different locations (indicated by black dashed lines) can interact with the beam to modulate the transition behavior. Notably, a larger design space is available for transition behavior modulation when CB is positioned closer to the fixed end. Thus we set the fixed starting point (represented by the brown dot in the figure) at $(w/H, h/H) = (0.18, 0.12)$, where $w$ and $h$ are normalized with respect to $W$ and $H$, respectively. It's noted that the end modulation strain is set to 0.5 to ensure that the structure retains a negative stiffness interval beyond the modulation range, enabling the transition to the other stable state. Additionally, an excessively long modulation interval compromises the regularity of the stress-strain curves.

We default set the parameters $H = 12$ mm, $W = 15$ mm, $t = 1.4$ mm, and out-of-plane thickness $b = 8$ mm and halve the parameters as the size of bistable units for grippers. It is worth noting that the stress and applied strain in the stress ($\sigma$)-strain ($\varepsilon$) curve of the bistable structure are converted from the force ($F$)-displacement ($d$) curves by the following formula:

$$\sigma = F/Wb, \varepsilon = d/2H \qquad \text{(S1)}$$

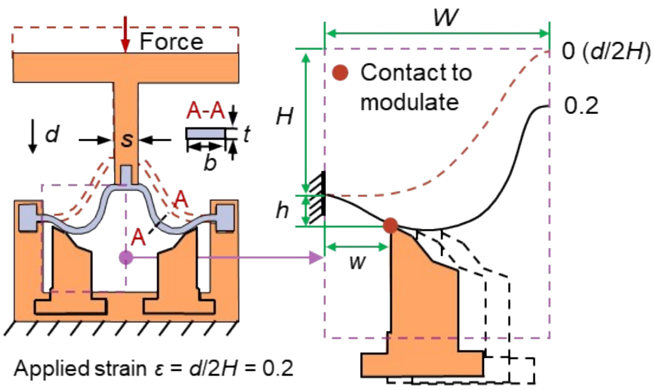


Fig. S1. The assembled bistable unit with CB to modulate the transition behavior.

The position, number, and shape of CB are demonstrated to significantly influence peak force, multiplateau, and local stiffness of transition behaviors, respectively (Fig. S2). By integrating these design strategies, we construct the parameterized CB model, i.e., a combination of different positions and inclinations (shapes) of three CBs. Specifically, the CB is determined by six geometrical parameters $w_1$, $w_2$, $w_3$, $h_1$, $h_2$, $h_3$.

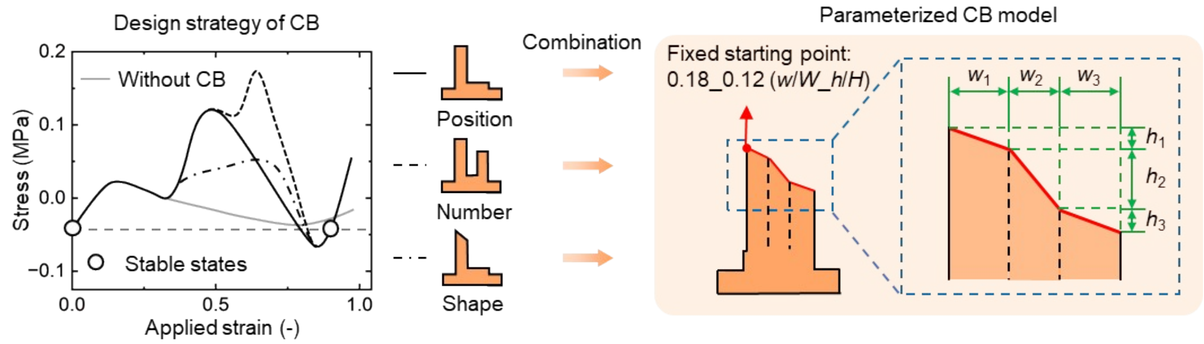


Fig. S2. The parameterized CB model constructed by combining three design strategies of CB.

## Section S2. Inverse design of CB model for target transition behaviors

### S2.1 The sampling of parameterized CB

The machine learning model requires sufficient training data to accurately predict the nonlinear transition behaviors of bistable units for arbitrary CB configurations. To generate such data, we first produce CB geometries using full factorial sampling. During the sampling process, we impose the conditions (Fig. S3) that (1) the width $w_s$ of CB is kept constant to prevent excessive local strains in the beams and avoid structural damage; (2) the modulation height difference $h_s$ of CB is constrained to avoid the loss of bistability; and (3) a specific value for $h_1$ is chosen to ensure effective modulation during the initial contact stage with CB. Furthermore, the geometrical parameters value ranges are as follows:

$$\begin{cases} 0.16W \le w_1 \le 0.29W, \\ 0.11W \le w_2 \le 0.19W, \\ 0.04W \le w_3 \le 0.44W, \\ 0.03H \le h_2 \le 0.22H, \\ 0 \le h_3 \le 0.37H, \end{cases} \tag{S2}$$

Wherein, the discrete intervals of the geometric parameter $w_1$, $w_2$, and $w_3$, are set to $0.03W$, while $h_2$ and $h_3$ are set to $0.02H$. Note that all geometric parameters are integer multiples of 0.1 mm to ensure compatibility with the printing process.

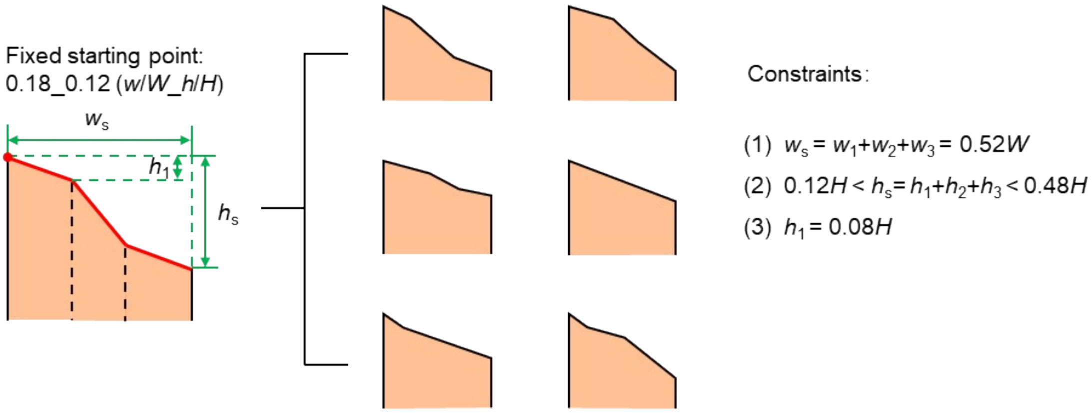


Fig. S3. Full factorial sampling based on some constraints.

### S2.2 The simulation setting to generate the dataset

We evaluate the transition behaviors of the generated CBs using Finite Element (FE) simulations conducted in the commercial finite element software ABAQUS. The deformation process is treated as quasi-static with surface-to-surface self-contacts implemented using the penalty method, assuming a friction coefficient of 0.6[2]. Geometric nonlinearity is accounted for, and the solver is stabilized using automatic stabilization with a dissipated energy fraction of 0.0001 and a maximum ratio of 0.01 relative to strain energy. The boundary condition of the bistable units is illustrated in Fig. S4a. The PLA material is represented as a high-modulus isotropic material, classified as 'rigid.' The lower section of the PLA material is fixed, while a displacement load of 24 mm is applied to its upper section. The TPU material is described using a two-parameter Mooney-Rivlin model, with $C_{10}$ = -0.54516, $C_{01}$ = 6.04727, $D_1$ = 0.001[1]. The TPU beam is meshed with hybrid formulation elements (element type: C3D8RH) while C3D8R elements are assigned to all other parts (Fig. S4b). As shown in Fig. 2c, we get 6720 stress-strain curves via numerical simulations.

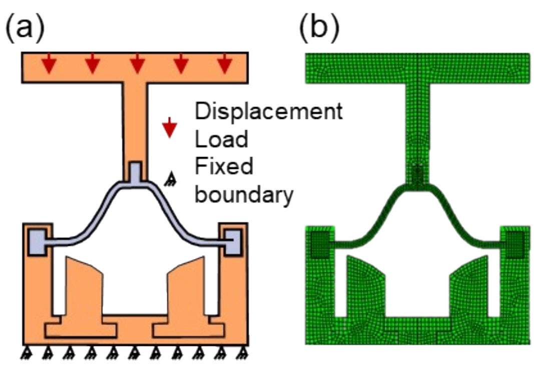


Fig. S4. (a) The boundary condition and (b) the discretized mesh model of the bistable units.

### S2.3 The training setting and robust verification of the ERT model

The stress-strain curves in the dataset can primarily be classified into two distinct types. As illustrated in Fig. S5, the first type exhibits a monotonic increase in stress with strain, potentially including a plateau region in the middle. The second type demonstrates an initial increase in stress, followed by a decrease after reaching the peak stress. In both cases, the characteristics of the stress-strain curves are straightforward to capture.

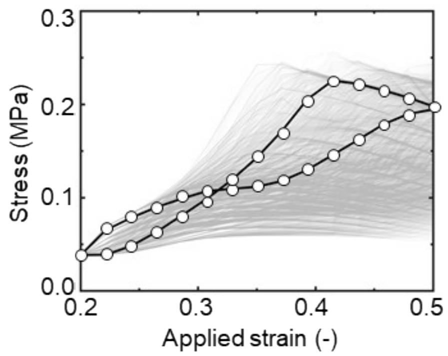


Fig. S5. The classical stress-strain curves of the built dataset.

To predict the lower-dimensional representation of the stress vector, $\boldsymbol{\sigma}_{\mathrm{CB}}$, for a given CB geometry, $\boldsymbol{X}_{\mathrm{CB}}$, an extremely randomized trees (ERT) model[3] is adopted. We randomly select $N_{\mathrm{tr}} = 0.8N$ data points for training, while the remaining $N_{\mathrm{test}} = 0.2N$ are reserved for testing. We train the ERT model parameters to minimize:

$$L = \frac{1}{N_{\mathrm{tr}}}\sum_{i=1}^{N_{\mathrm{tr}}} err\,(\boldsymbol{\sigma}_{\mathrm{CB}}^{i}), \tag{S3}$$

$err\,(\boldsymbol{\sigma}_{\mathrm{CB}}^{i})$ is the same as Formula 2 in the manuscript. The training is performed using the following parameters:

- n_estimators: 200
- min_samples_split: 2
- max_features: 1
- max_depth: None
- min_samples_split: 2
- Bootstrap: False

Among them, the stability of the model improves as the number of estimators (n_estimators) increases. However, this also results in longer training and prediction time. When utilizing 500 estimators to train the model, the computation time is more than half that required for 200 estimators, while the improvement in model accuracy remains minimal.

The robustness of the trained ERT model is further assessed using the test data. The parameterized CB in the test set includes both types of transition behaviors, covering a range of parameter values, including boundary values (specific parameters are listed in Table S1), as shown in Fig. S6. The prediction results of the ERT model align well with the simulation results, demonstrating the model's strong robustness across different geometric configurations.

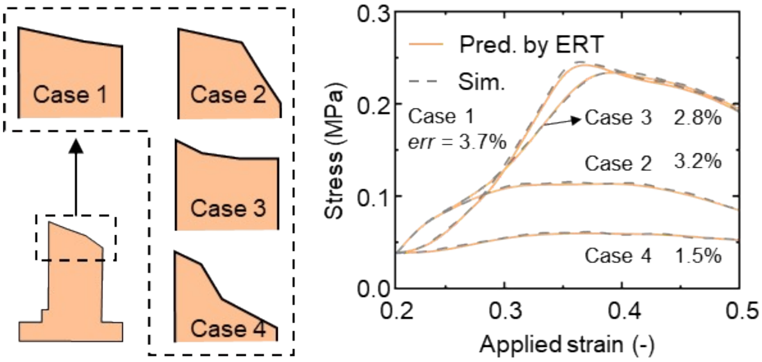


Fig. S6. Different geometric shapes and stress-strain curves of parameterized CB in the test set.

Table S1. The geometrical parameters of the parameterized CB

| geometrical parameters | $w_1/W$ | $w_2/W$ | $w_3/W$ | $h_1/H$ | $h_2/H$ | $h_3/H$ |
|---|---|---|---|---|---|---|
| Case 1 | 0.32 | 0.19 | 0.01 | 0.08 | 0.03 | 0.00 |
| Case 2 | 0.32 | 0.11 | 0.09 | 0.08 | 0.22 | 0.18 |
| Case 3 | 0.13 | 0.19 | 0.20 | 0.08 | 0.03 | 0.00 |
| Case 4 | 0.13 | 0.11 | 0.28 | 0.08 | 0.22 | 0.18 |

### S2.4 The optimization framework to achieve the inverse design of the CB model

As shown in Fig. S7, four target points on the stress-strain curves are selected to define the target linear stiffness behaviors. The objective is to minimize the mean square error between the experimental stress of the current CB and the target linear stiffness at these four points. The residual $r_i$ at the $i$-th target point is defined as $(\sigma_{\exp}^{i} - \sigma_{\mathrm{tar}}^{i})^2$. Consequently, the complete mathematical formula of this geometry optimization problem can be expressed as follows:

$$\begin{aligned} &\text{Find} \quad w_1, w_2, w_3, h_2, h_3 \\ &\text{Min.} \quad \mathrm{MSE} = \frac{1}{4}\sum_{i=1}^{4} r_i \\ &\text{S.t.} \quad \begin{cases} w_1 + w_2 + w_3 = 0.52W \\ 0.12H < h_2 + h_3 < 0.48H \end{cases} \end{aligned} \tag{S4}$$

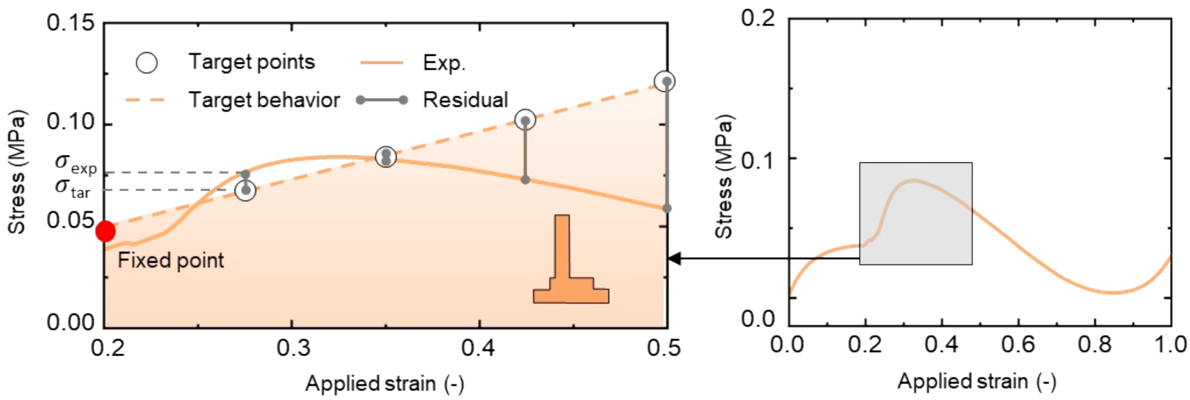


Fig. S7. The objective function is defined as the error between the experimental stress from the current CB and the target linear stiffness at four points.

Based on the trained ERT model, we couple with the Differential Evolution (DE) algorithm[4] to implement the inverse design process. The optimization process is performed using the following parameters. The number of populations of each generation is determined by multiplying the population size by the number of variables. In this case, with four free variables, the total population size of each generation is 60.

- Strategy: 'best1bin'
- Population size: 15
- Mutation: (0.5, 1)
- Maximum iteration: 100
- Tolerance: 0.01
- Recombination: 0.7

We use the target linear stiffness $\sigma = 0.24\varepsilon$ MPa as an example. The optimal and verification results are illustrated in Fig. S8. During the optimization process, the objective function, represented by MSE, converges to 0.4%. Furthermore, numerical simulations and experimental tests validate the effectiveness of the inverse design method.

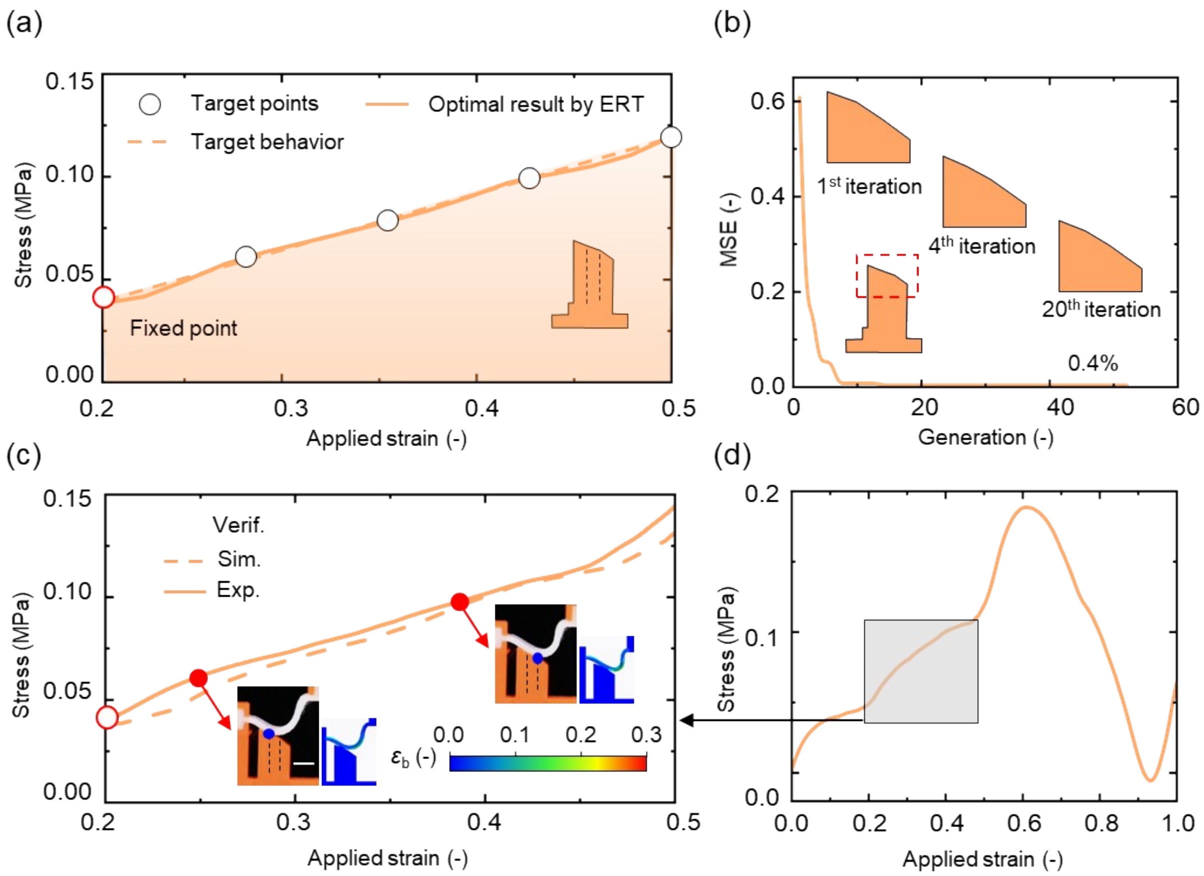


Fig. S8. Demonstration and verification of the inverse design method based on the target linear stiffness $\sigma = 0.24\varepsilon$ MPa. (a) Comparison of the target behavior and the optimal result. (b) Iterations of objective function MSE for obtaining the designed CB. (c) Simulation and experimental verification of the transition behaviors of the designed CB.

Table S2. The geometrical parameters of the designed CB corresponding to target linear stiffness $\sigma = 0.24\varepsilon$ MPa

| Stiffness behavior | $w_1/W$ | $w_2/W$ | $w_3/W$ | $h_1/H$ | $h_2/H$ | $h_3/H$ |
|---|---|---|---|---|---|---|
| $k = 0.24$ | 0.18 | 0.16 | 0.18 | 0.08 | 0.10 | 0.17 |

**Section S3. Soft-rigid grippers comprising pixel arrays of bistable units**

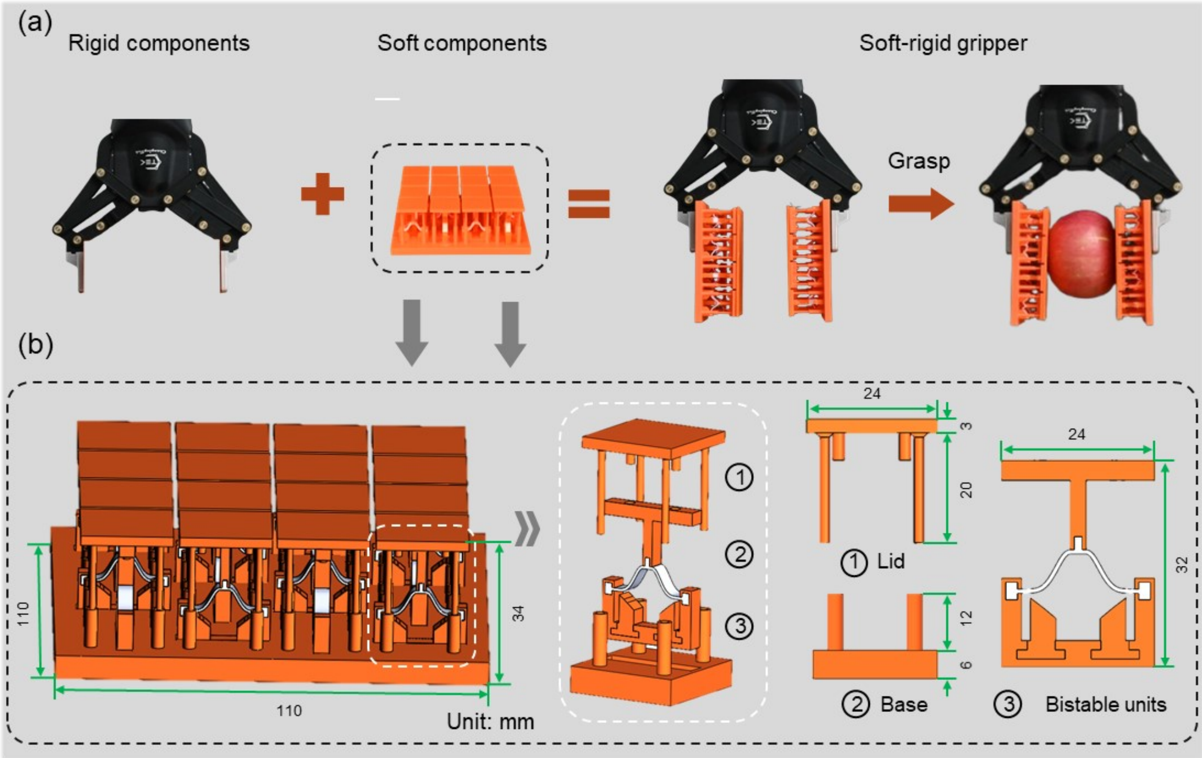


Fig. S9. (a) The individual components of soft-rigid grippers, scale bar: 20 mm. (b) The design details of the soft component comprising pixel arrays of bistable units.

The samples were fabricated using an Ultimaker S5 3D printer (Ultimaker B.V., Utrecht, The Netherlands) with a dual-material extrusion method, depositing layers sequentially (Fig. S10a). PLA (Polymaker, China) was extruded through Nozzle 1, while TPU (Polymaker, China) was extruded through Nozzle 2. The nozzle diameter is 0.4 mm, and the layer height in the Z direction is 0.1 mm. As shown in Fig. S10b, the bistable unit parameters are scaled to half the size of those in Fig. S1, with key dimensions of $H = 6$ mm, $W = 7.5$ mm, $t = 0.8$ mm, and $b = 4$ mm. The bistable units are primarily secured to the base through an interference fit, while the soft components and rigid components are bonded using elastomer glue.

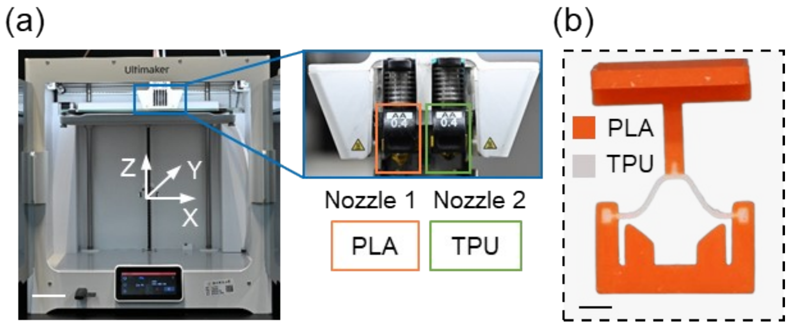

Fig. S10. (a) 3D printer for printing samples, scale bar: 80 mm. (b) Printed samples with two materials, scale bar: 5 mm.

The grasping strategy is illustrated in Fig. S11. Specifically, we preconfigure interconnected bistable units, ensuring that, upon contact with an object, the loaded units exhibit the same displacement *d*. Based on the force-displacement curves of the bistable units, we estimate the force applied to the objects. Given the specific friction coefficient of the contact surface, the grasping force *F* is subsequently obtained. For deformable objects, we add integrated displacement sensors into the units to determine the displacement of the bistable units, allowing for precise determination of the grasping force. We test that for bistable units with the high stiffness behavior design, the lift-weighting capability of the gripper is 1200 g before undergoing snap-through behavior.

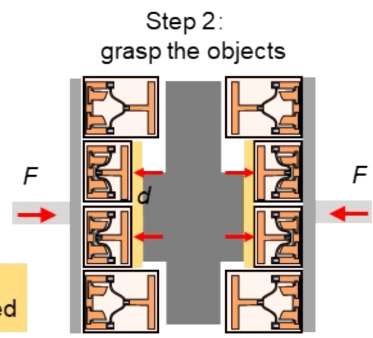

Fig. S11. Schematic diagram of the grasping strategy.

**Section S4. Determination of grasping behaviors for soft-rigid grippers**

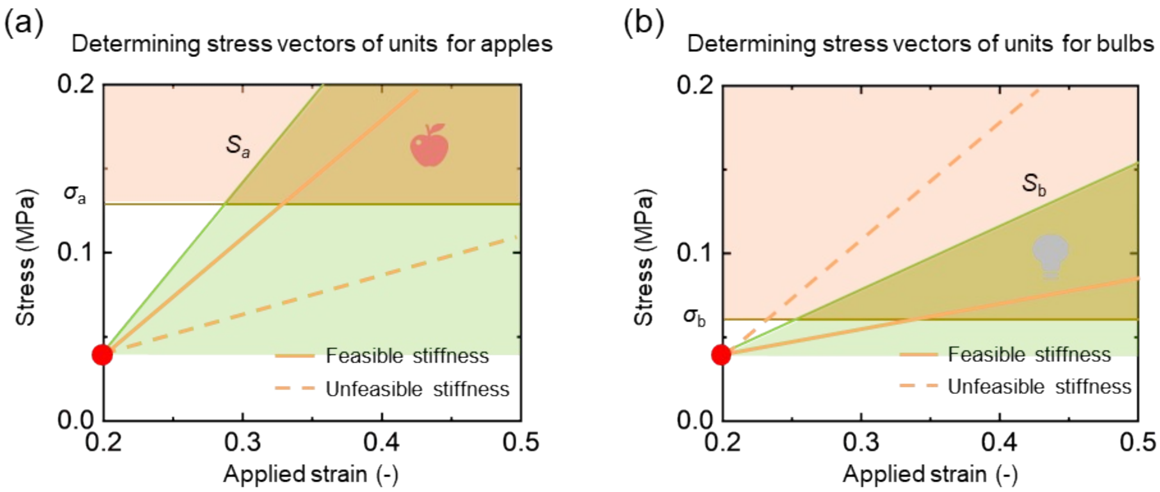


Fig. S12. Determining feasible stress vectors of bistable units for various objects, e.g., (a) apples, $\sigma_a = 0.13$ MPa, and $S_a = 0.8$ mm/N. (b) bulbs, $\sigma_b = 0.06$ MPa, and $S_b = 2.0$ mm/N.

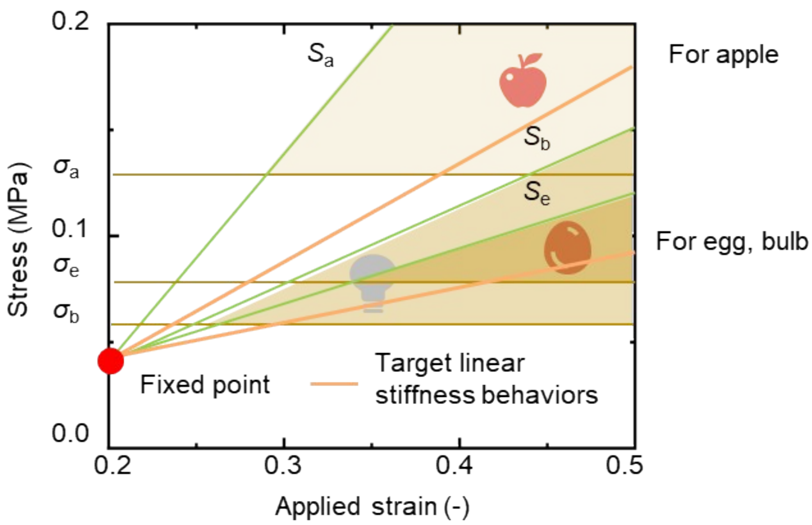


Fig. S13. Determining the target linear stiffness behaviors for grasping various objects. The low stiffness behavior, $\sigma = 0.16\varepsilon + 0.02$ MPa, is ideal for grasping the safety-first egg and bulb. While the high stiffness behavior, $\sigma = 0.40\varepsilon - 0.03$ MPa, is suited for grasping the apple.

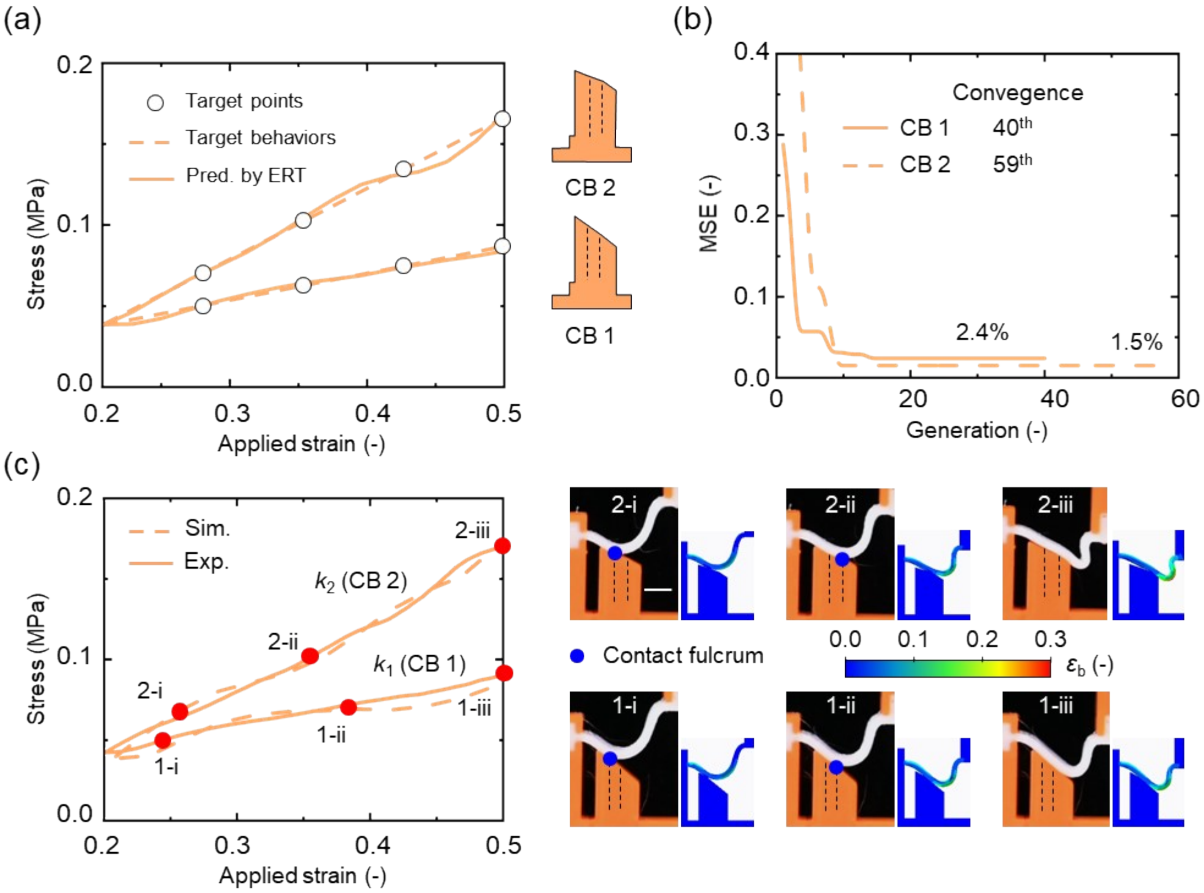


Fig. S14. Design details of CB corresponding to target linear stiffness behaviors, i.e., the low linear stiffness behavior, $\sigma = 0.16\varepsilon + 0.02$ MPa, and the high stiffness behavior, $\sigma = 0.40\varepsilon - 0.03$ MPa. (a) Comparison of target behaviors with optimized results obtained by the trained ERT model. (b) Iterations of objective function MSE for obtaining the designed CB. (c) Simulation and experimental verification of the transition behaviors of the designed CB.

Table S3. The geometrical parameters of designed CB corresponding to target linear stiffness behaviors

| Stiffness behavior | $w_1/W$ | $w_2/W$ | $w_3/W$ | $h_1/H$ | $h_2/H$ | $h_3/H$ |
|---|---|---|---|---|---|---|
| $k_1$ (CB 1) | 0.13 | 0.14 | 0.25 | 0.08 | 0.13 | 0.27 |
| $k_2$ (CB 2) | 0.19 | 0.18 | 0.15 | 0.08 | 0.08 | 0.13 |

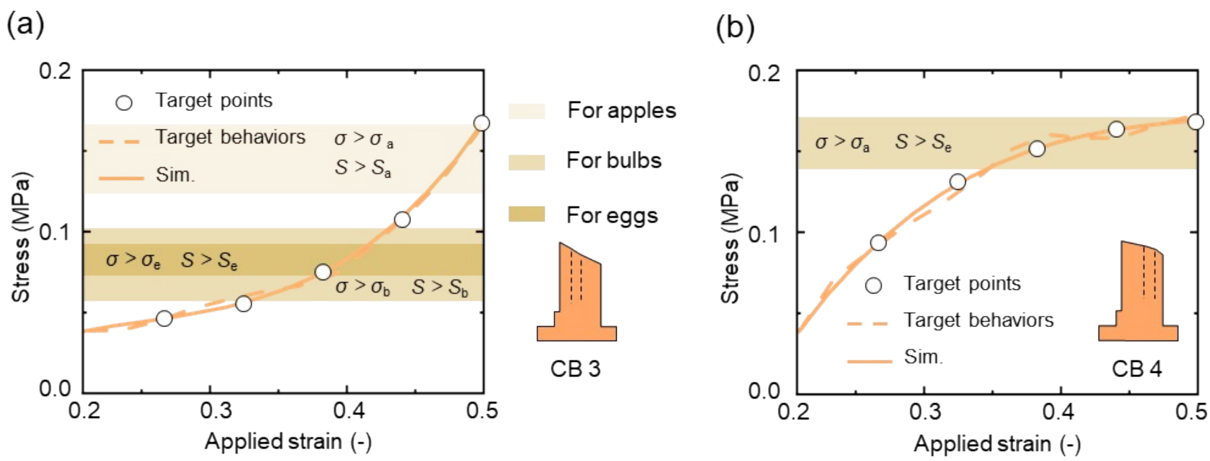


Fig. S15. Multi-trait behaviors for fulfilling more object-grasping tasks. (a) Concave behaviors for grasping apples, eggs, and bulbs (heavy and rigid, light and fragile). (b) Convex behaviors for grasping objects that are heavy and fragile, e.g., objects with $\sigma_a$ and $S_e$.

Table S4. The geometrical parameters of the designed CB corresponding to multi-trait behaviors

| Multi-trait behavior | $w_1/W$ | $w_2/W$ | $w_3/W$ | $h_1/H$ | $h_2/H$ | $h_3/H$ |
|---|---|---|---|---|---|---|
| Concave (CB 3) | 0.13 | 0.12 | 0.27 | 0.08 | 0.10 | 0.16 |
| Convex (CB 4) | 0.31 | 0.11 | 0.09 | 0.08 | 0.04 | 0.09 |

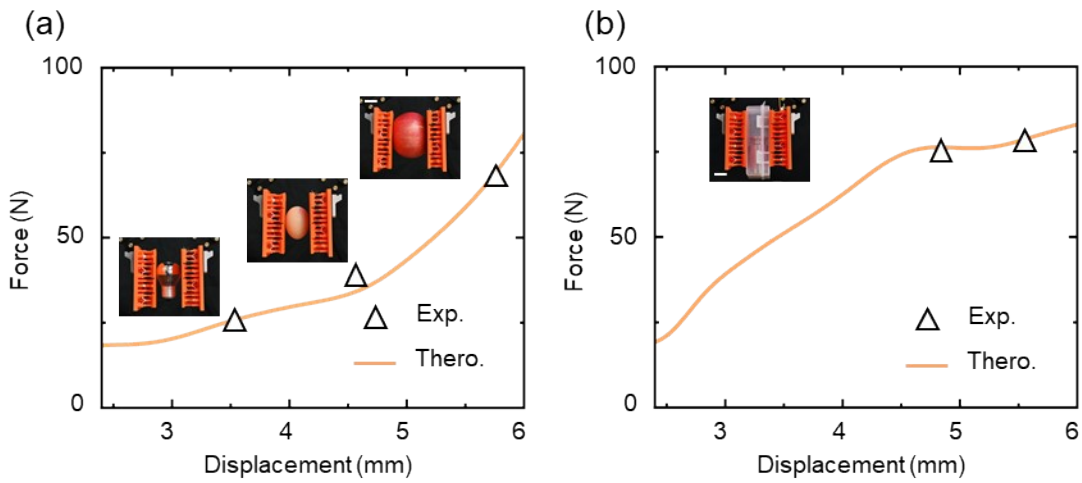


Fig. S16. Experimental validation of (a) concave and (b) convex grasping behaviors, scale bar: 20 mm. The theoretical curve is derived from the superposition of numerical simulation results of the designed units.

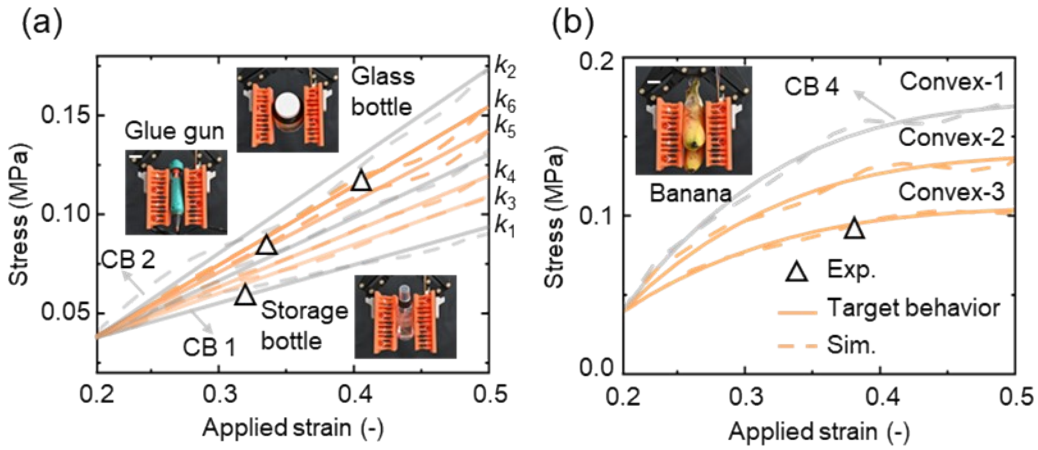


Fig. S17. Design and experimental verification of (a) various linear stiffness and (b) convex behaviors, scale bar: 20 mm. The required stress and compliance of objects are as follows: glue gun: $\sigma$ = 0.07 MPa, $S$ = 0.1 mm/N; glass bottle: $\sigma$ = 0.12 MPa, $S$ = 1.0 mm/N; storage bottle: $\sigma$ = 0.05 MPa, $S$ = 2.1 mm/N; banana: $\sigma$ = 0.07 MPa, $S$ = 3.2 mm/N.

Table S5. The geometrical parameters of the designed CB corresponding to various linear stiffness and convex behaviors. (The geometric parameters of $k_1$ and $k_2$ transition behavior are shown in Table S3)

| Transition behavior | $w_1/W$ | $w_2/W$ | $w_3/W$ | $h_1/H$ | $h_2/H$ | $h_3/H$ |
|---|---|---|---|---|---|---|
| $k_3$ | 0.16 | 0.17 | 0.19 | 0.08 | 0.13 | 0.19 |
| $k_4$ | 0.17 | 0.16 | 0.19 | 0.08 | 0.11 | 0.18 |
| $k_5$ | 0.18 | 0.17 | 0.17 | 0.08 | 0.09 | 0.16 |
| $k_6$ | 0.19 | 0.18 | 0.15 | 0.08 | 0.09 | 0.13 |
| Convex-2 | 0.27 | 0.11 | 0.15 | 0.08 | 0.05 | 0.17 |
| Convex-3 | 0.21 | 0.11 | 0.20 | 0.08 | 0.08 | 0.23 |

## Reference


[1] J. He, Y. Wang, Z. Shen, L. Xia, Y. Xiong, *Mater. Horizons* **2024**, DOI 10.1039/d4mh00906a.

[2] R. Elleuch, K. Elleuch, H. Ben Abdelounis, H. Zahouani, *Mater. Sci. Eng. A* **2007**, *465*, 8.

[3] P. Geurts, D. Ernst, L. Wehenkel, *Mach. Learn.* **2006**, *63*, 3.

[4] A. Qing, *Differ. Evol. Fundam. Appl. Electr. Eng.* **2009**, 1.